International Journal of Mechanical and Electrical Engineering
ISSN: 3005-9615 (Print), ISSN: 3005-7132 (Online) | Volume 2, Number 3, Year 2024
DOI: https://doi.org/10.62051/ijmee.v2n3.12
Journal homepage: https://wepub.org/index.php/IJMEE/index

Multi-objective Optimization Design of Six-phase U-shaped Permanent Magnet Linear Vernier Motor

Yugang Jin, Xiaozhuo Xu *

School of Electrical Engineering and Automation, Henan Polytechnic University, Jiaozuo, China
* Corresponding Author: Xiaozhuo Xu

ABSTRACT

For the cordless hoisting system, a six-phase U-shaped permanent magnet linear vernier motor (SU-PMLVM) is proposed. The primary of the motor adopts a U-shaped segmented permanent magnet array, which is characterized by a high magnetization effect and a low magnetic leakage. In order to enhance the comprehensive performance of SU-PMLVM, the average thrust, thrust fluctuation, and no-load counter potential harmonic distortion rate are selected as optimization objectives. Taguchi's method is employed to expeditiously optimize SU-PMLVM in a multi-objective manner. Firstly, the optimization variables with the greatest influence on the objectives and the values of their factor levels are selected. Then, the designed orthogonal experiments are solved by using the finite element method, and the performance data of each optimization objective under different combinations of factor levels are obtained. Finally, the influence weights of the optimization variables in each optimization objective are clarified through the analysis of variance, and the optimal level combinations of the optimization variables are thus obtained. A comparison of the performance of the objectives before and after optimization indicates that the average thrust of the proposed motor has increased by 1.77%, the thrust fluctuation has been reduced by 40.06%, and the no-load reverse potential harmonic distortion rate has been reduced by 15.23%.

KEYWORDS

Six-Phase U-Shaped Permanent Magnet Linear Vernier Motor; Finite Element Method; Taguchi Method; Multi-Objective Optimization.

1. INTRODUCTION

Permanent-magnet linear vernier motor (PMLVM) not only possesses the characteristics of high efficiency, high power factor, and large thrust density at low speed, but also is favored for its simple structure and rapid dynamic response, and is one of the drive sources with significant advantages in the fields of long-stroke cordless lifting and rail transportation under complex working conditions [1-3].

In order to meet the urgent demand for large thrust performance and low permanent magnet cost of PMLVMs, scholars at home and abroad have devoted extensive attention to studies on improving the thrust density and permanent magnet utilization of motors[4]. These studies primarily focus on the innovation or optimization of topological structures, such as the multi-tooth split-pole structure and permanent magnet optimization[5-6]. In a previous study, a primary permanent magnet vernier linear motor with an N-S pole structure was proposed, which demonstrated the ability to generate higher thrust at low speeds through the utilization of the "magnetic gearing effect" [7]. In a related study, literature [8] proposed a V-type permanent magnet vernier permanent magnet linear motor. Each pole consists of two identical rectangular permanent magnets and a triangular convex iron pole, which

exhibits a certain degree of magnetization. This configuration has the potential to enhance the air-gap magnetic density waveform and thrust density of the motor. In [9], a polymagnetized permanent magnet vernier linear motor was proposed, which employs Halbach permanent magnet arrays on the surface of the secondary teeth of the motor to reduce edge leakage. A prototype was fabricated, which demonstrated that this structure has the advantage of high thrust density, but also exhibited end effects. In a subsequent publication, Literature [10] proposed a modular fault-tolerant permanent magnet vernier linear motor. This motor employs a multiphase and modular design to enhance the fault-tolerance of the motor, and optimizes the permanent magnet charging direction to improve thrust performance.

Although PMLVM has the advantage of high thrust density, it also has the problems of high thrust fluctuation and more magnetic leakage. Therefore, it is necessary to carry out multi-objective optimization of the motor. The difficulties of multi-objective optimization lie in the relative complexity of the operation principle of PMLVM, the time-consuming finite element analysis, and the conflict between design variables and optimization objectives. To address these issues, a number of optimization algorithms are commonly employed in the multi-objective optimization design of electric motors, including the particle swarm optimization algorithm, genetic algorithm, and Taguchi method, among others. These algorithms have a wide range of applications in the field of electric motor design. They are capable of effectively dealing with the complex relationship between multiple optimization objectives and of finding the optimal solution to meet the design requirements. In literature [11], the finite element method was employed to optimize a miniature linear rotary voice coil motor, with output torque and torque fluctuation serving as the optimization objectives. Literature [12] utilized the response surface method to optimize the structure of a built-in external rotor type permanent magnet motor utilized in hoists. The literature [13] presents a particle swarm algorithm-based approach to multi-objective optimization for the design of switched reluctance motors. This method effectively improves the utilization and stability of permanent magnets in the system. The literature [14-15] describes the optimization of motor control and body designs, respectively, using a genetic algorithm. Taguchi's method is an efficient multi-objective optimization method that requires less model arithmetic than other algorithms and avoids the complex algorithm derivation process. The method is based on orthogonal experimental design and signal-to-noise ratio technology, which can effectively optimize multiple objectives and obtain the best combination of each design parameter. Among these, the use of orthogonal experimental design can significantly reduce the number of experiments and improve the optimization efficiency [16-17]. Therefore, the Taguchi method has high practical value in practical engineering applications.

This paper proposes a six-phase U-shaped permanent magnet linear vernier motor (SU-PMLVM), which is distinguished by its high thrust, robust fault tolerance, minimal thrust fluctuation, and low harmonic distortion rate of no-load reverse potential. Section 2 provides an overview of the structure and operation principle of the SU-PMLVM. Section 3 employs Taguchi's method to perform multi-objective optimization of the SU-PMLVM, with the objective of further enhancing the comprehensive motor performance. Finally, Section 4 offers a summary and conclusion of the paper.

2. MOTOR STRUCTURE AND OPERATION PRINCIPLE

2.1. Motor Structure

The structure of the established six-phase Halbach-shaped permanent magnet linear vernier motor (SH-PMLVM) is depicted in Fig.1(a) [10], which comprises three distinct components: a brief primary, an air gap, and a lengthy secondary. The primary encompasses a primary core, armature windings, and permanent magnet arrays, whereas the secondary is constituted solely of silicon steel sheets. The structure of the SU-PMLVM, as proposed in this paper, is depicted in Fig.1(b). The SU-PMLVM maintains the same structural parameters as the SH-PMLVM, including the amount of

permanent magnets, the primary pole pitch, the secondary tooth width, the secondary tooth height, and the armature winding turns and wires. However, it differs from the SH-PMLVM in that it maintains the same rated current and the same rated speed of the primary as that of the SH-PMLVM. The Halbach poles in the SH-PMLVM are replaced with U-shaped permanent magnet arrays in order to reduce magnetic leakage and improve thrust performance. Fig.2 shows a comparison of the magnetic field distributions of the two motors, and it can be seen that there is less magnetic leakage at the pole edges of the SU-PMLVM. The armature winding of this motor is centrally wound, with one coil over each primary tooth. This structure results in shorter winding ends, lower copper consumption, and reduced physical contact between phases, which provides better fault-tolerance performance. Figures 3 and 4 show the 3D structure and basic dimensions of the proposed motor, respectively, and the parameters of the permanent magnet structure of the two motors are shown in Table 1.

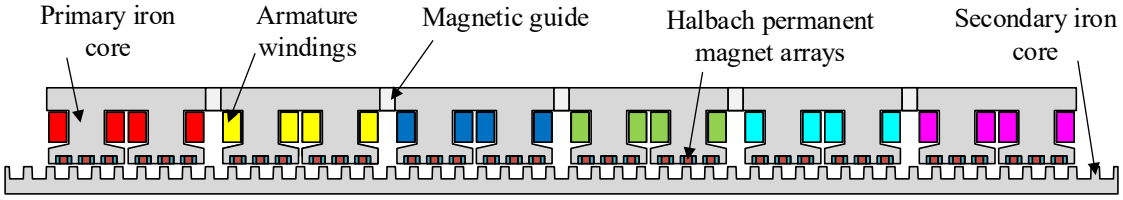

(a) SH-PMLVM cross-section

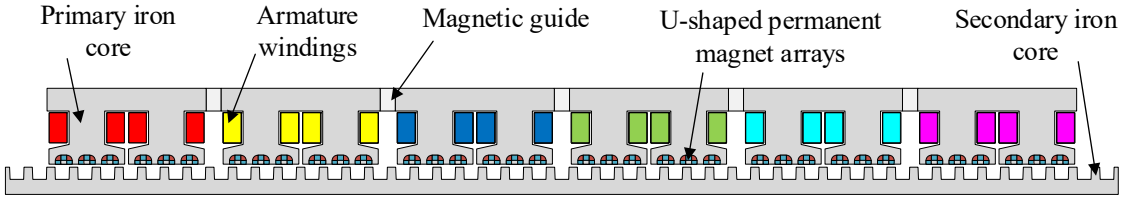

(b) SU-PMLVM cross-section

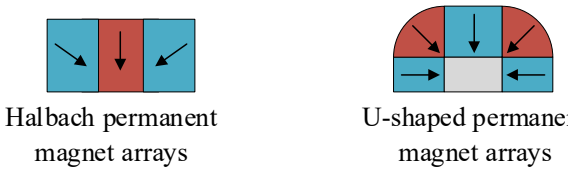

(c) Permanent magnet arrays

Figure 1. Comparison of the structure of two motors

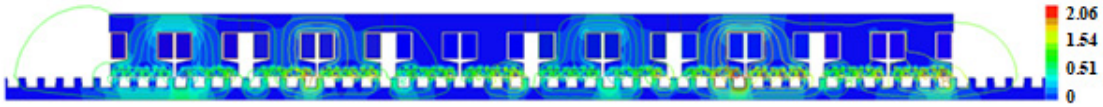

(a) SH-PMLVM Magnetic Field Distribution

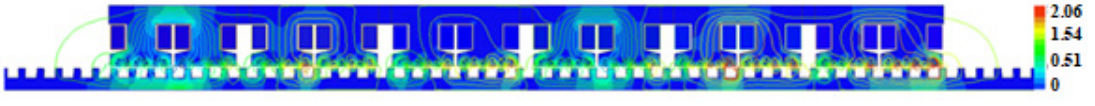

(b) SU-PMLVM Magnetic Field Distribution

Figure 2. Magnetic Field Distribution Comparison

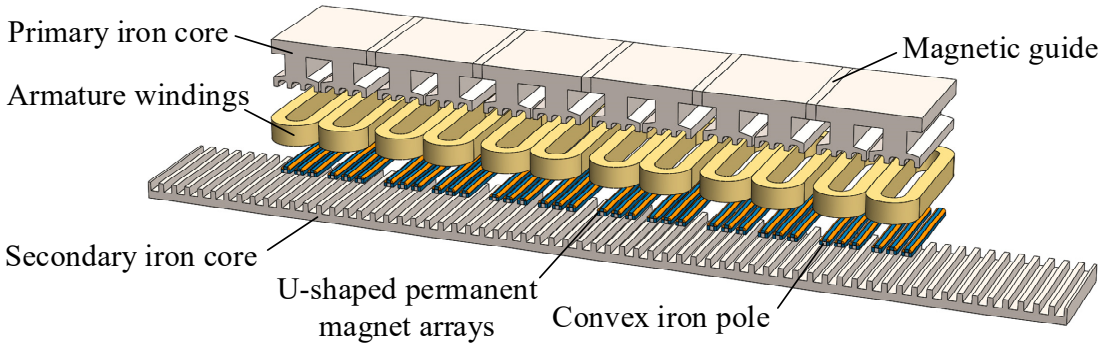

Figure 3. SU-PMLVM 3D Exploded Drawing

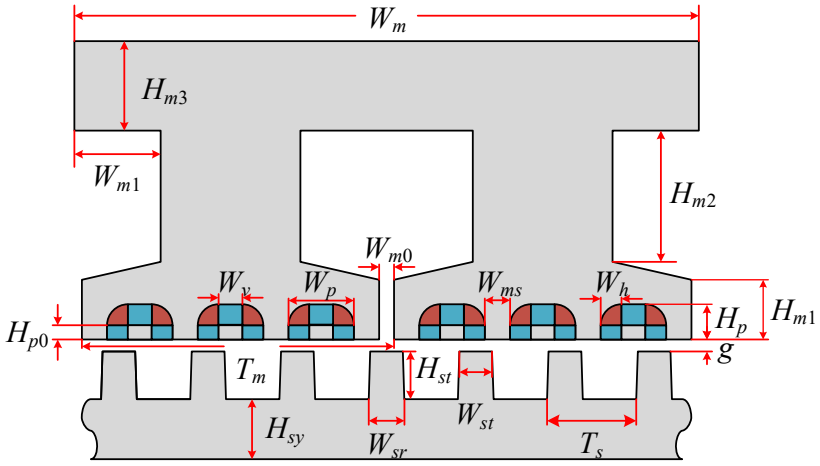

Figure 4. Basic Dimensions Of The Motor

Table 1. Motor Permanent Magnet Structure Parameters

Parameters (mm)	SH-PMLVM	SU-PMLVM
Horizontal magnetizing PM height /H_{p0}	5	2.4
Vertical magnetizing PM width /W_v	3	4
Total magnet width /W_p	10	11
Oblique magnetizing PM width /W_h	3.5	3.5
Primary split tooth width /W_{ms}	5	4.25

2.2. Principle of Motor Operation

In order to ensure stable operation of the motor, it is necessary to ensure that the secondary winding magnetic field pole pair and speed are equal to the magnetic field pole pair and speed generated by the permanent magnet [18]. This can be achieved by ensuring that the permanent magnet pole pair Ppm, the armature winding pole pair Pw, and the secondary effective number of teeth Ns satisfy the relation equation (1-3).

$$N_s = \left| P_{pm} \pm P_w \right| \cdot \tag{1}$$

The motor speed is found to satisfy the following conditions.

$$v_{pm} = \frac{P_w}{P_{pm}} v \,. \tag{2}$$

$$G = \frac{P_w}{N_s} \,. \tag{3}$$

The linear velocity of the primary, denoted by v, is the velocity of the magnetic field generated by the permanent magnet, which is represented by v_{pm}. The vernier effect coefficient, represented by G, is a constant that is used to calculate the velocity of the magnetic field.

In the SU-PMLVM proposed in this paper, the 42 effective secondary teeth in the secondary section modulate with the 6-pole armature magnetic field generated by the armature windings on the primary. This generates a 36-pole magnetic field in the air gap, which interacts with the effective 36-pole permanent magnet magnetic field on the primary to boost the thrust.

3. SU-PMLVM MULTI-OBJECTIVE OPTIMIZATION

3.1. Optimization Methodology and Objectives

Due to the numerous optimization objectives of the motor and the presence of constraints, the utilization of Taguchi's method can minimize the number of experiments while ensuring the optimization effect is achieved and facilitate the rapid multi-objective optimization of the SU-PMLVM. The multi-objective optimization flow of the SU-PMLVM is depicted in Fig.5.

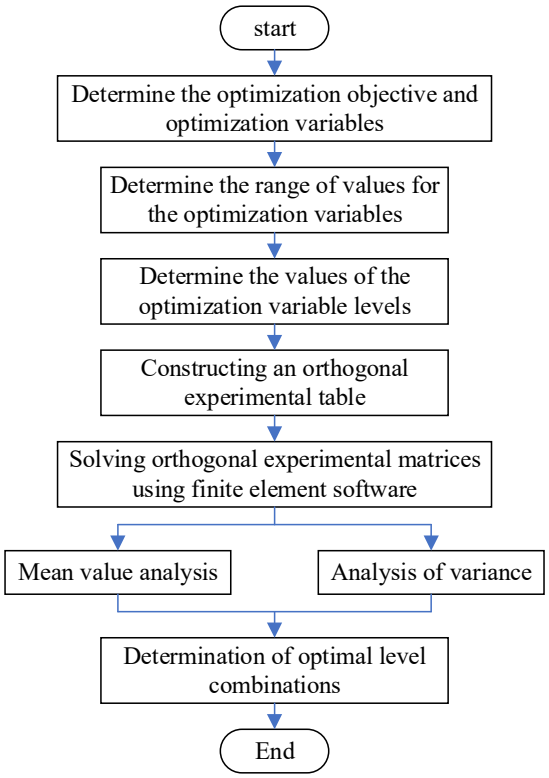

Figure 5. Taguchi's Method Of Optimizing Processes

Given that the primary teeth modulate the coupling of the armature magnetic field and the excitation magnetic field to produce a stable thrust output, it can be seen that the differences in the structural parameters of the permanent magnets and the secondary teeth have an important effect on the magnetic field modulation effect. In this paper, the average motor thrust (F_{avg}), thrust fluctuation (K_R), and no-load counter potential harmonic distortion rate (K_T) are taken as the optimization objectives. Four structural parameters are selected for the analysis: pole transverse occupancy ratio (a), primary notch height (b), secondary tooth height (c), and secondary tooth pole-arc coefficient (d). Among these parameters, a is the ratio of the obliquely magnetized PM width W_h to the total width of the magnet W_p, b is the primary notch height H_{m1}, c is the secondary tooth height H_{st}, and d is the ratio of the secondary tooth tip width W_{st} to the secondary pole pitch T_s.

Thrust fluctuation K_R reflects the degree of fluctuation of the motor thrust waveform and is defined as:

$$K_R = \frac{F_{\max} - F_{\min}}{F_{avg}} \times 100\% . \tag{4}$$

Where $F_{\max}$, $F_{\min}$ and F_{avg} are the maximum, minimum and average values of the motor thrust, respectively.

The no-load counter potential harmonic distortion rate K_T reflects the degree of no-load counter potential sinusoidality and is calculated as follows:

$$THD = \frac{\sqrt{E_2^2 + E_3^2 + \cdots + E_9^2}}{E_1} . \tag{5}$$

where E_i is each harmonic.

By analyzing the effect of these four structural parameters on the thrust performance of the motor, while keeping the other structural parameters of the motor unchanged, the relationship between the optimized target performance of the motor and the variation of each parameter is shown in Figures 6 and 7.

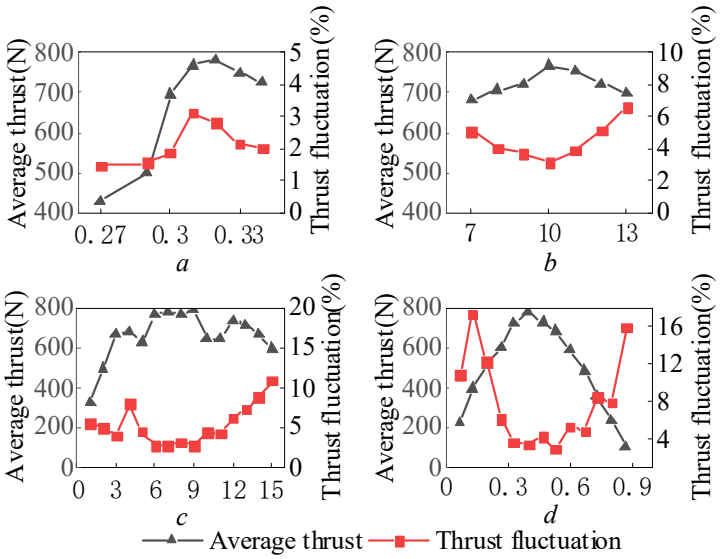

Figure 6. Effect Of Parameter Variation On Motor Thrust Performance

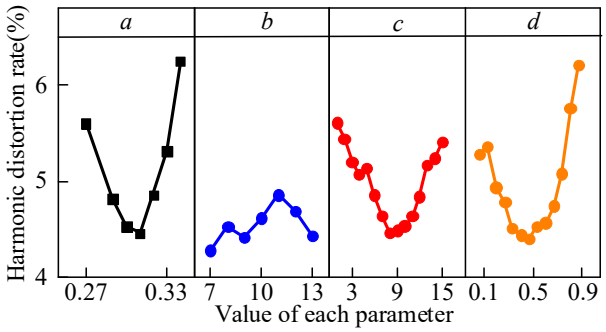

Figure 7. Influence Of Parameter Variations On The Harmonic Distortion Rate Of No-Load Counter Potentials

From the trend of the target performance with the parameters in Fig.6 and Fig.7, the parameter *b*, which has less influence on the optimized target performance, can be eliminated, and the optimization variables are selected as parameters *a*, *c*, and *d*. The level settings of each optimization variable are shown in Table 2.

Table 2. Factor Level Settings

Parameters	*a*	*c*/mm	*d*
Level 1	0.29	5	0.23
Level 2	0.3	6	0.3
Level 3	0.31	7	0.37
Level 4	0.32	8	0.43
Level 5	0.33	9	0.5

3.2. Orthogonal Experiment

Table 3. Orthogonal Experimental Program And Results

Test	*a*	*c*	*d*	F_{avg}/N	K_R/%	K_T/%
1	0.29	5	0.23	540.68	2.07	5.14
2	0.29	6	0.3	560.72	1.03	5.47
3	0.29	7	0.37	673.46	1.57	6.18
4	0.29	8	0.43	668.16	1.6	4.12
5	0.29	9	0.5	655.76	1.34	4.74
6	0.3	5	0.3	766.14	2.83	5.19
7	0.3	6	0.37	787.93	2.76	5.38
8	0.3	7	0.43	788.16	1.17	4.37
9	0.3	8	0.5	784.12	2.47	4.67

Continued Table

Test	*a*	*c*	*d*	F_{avg}/N	K_R/%	K_T/%
10	0.3	9	0.23	762.55	1.6	3.70
11	0.31	5	0.37	772.86	7.06	4.54
12	0.31	6	0.43	795.9	5.01	4.90
13	0.31	7	0.5	790.91	2.86	5.34
14	0.31	8	0.23	747.19	4.92	4.05
15	0.31	9	0.3	768.42	2.67	5.22
16	0.32	5	0.43	739.45	13.14	5.67
17	0.32	6	0.5	790.34	3.36	4.15
18	0.32	7	0.23	711.74	2.82	4.22
19	0.32	8	0.3	796.88	4.96	4.60
20	0.32	9	0.37	812.82	3.48	5.35
21	0.33	5	0.5	781.76	4.24	4.43
22	0.33	6	0.23	604.44	1.83	4.67
23	0.33	7	0.3	804.55	2.14	4.45
24	0.33	8	0.37	799.16	2.67	4.43
25	0.33	9	0.43	769.86	2.93	4.49

If a full factorial experiment is conducted on the designed three-variable, five-level optimization scheme, a total of 5^3=125 experiments must be conducted, the total optimization time is long, and the experiment is difficult. By using orthogonal experimental design, only 5^2=25 experiments need to be conducted, which greatly reduces the number of experiments and improves the overall efficiency of the optimization scheme. Table 3 shows the table of orthogonal experiments of the optimization scheme in this paper and the optimization objective values corresponding to each experiment.

The overall average of all trials is calculated, where X_{avg} is the overall average of each optimization objective, and the results are shown in Table 4.

Table 4. Total Average Of Motor Optimization Objectives

Average value	F_{avg}/N	K_R/%	K_T/%
X_{avg}	738.96	3.30	4.78

To determine the effect of each optimization variable on the motor's average thrust F_{avg}, thrust fluctuation K_R, and no-load harmonic distortion K_T, the average values of these three optimization variables at each level are calculated as follows:

$$X_{\delta(l)} = \frac{1}{n}\left[x_\delta(s) + ... + x_\delta(w)\right]. \tag{6}$$

Where, $X_{\delta(l)}$ denotes the average value of the optimization objective under the lth level factor of parameter x, δ is a, c and d waiting for the optimization variables; $X_{\delta(s)}$ is the value of a certain optimization objective under the sth experiment under the lth level factor of parameter x; n is the number of level of each optimization variable selected in the optimization scheme, and in this paper, n=5; s, w are the experimental sequence numbers. For example, calculate the average thrust of the motor when the level of parameter a factor is 1 as an example, $A_{Favg\,(1)}$, the calculation is shown in equation (7).

$$A_{F_{avg}(1)} = \frac{1}{5}\left[a_{F_{avg}}(1) + a_{F_{avg}}(2) + a_{F_{avg}}(3) + a_{F_{avg}}(4) + a_{F_{avg}}(5)\right]. \tag{7}$$

The average performance for each optimization objective is calculated and shown in Figure 8. From Fig.8, it can be seen that as the factor level of parameter a increases, the average thrust and thrust fluctuation have a large value; for parameter c, as the factor level increases, the three optimization objectives have a very small value; for parameter d, as the factor level increases, the three optimization objectives have a large value. When the value of parameter factor is optimally determined with a single optimization objective, when the value of parameter factor is $a(3)c(4)d(4)$, the average thrust F_{avg} is the largest; when the value of parameter factor is $a(2)c(3)d(3)$, the thrust fluctuation K_R is the smallest; and when the value of parameter factor is $a(1)c(3)d(1)$, the no-load counter potential harmonic distortion rate K_T is the smallest. In summary, it can be seen that the motor optimization objectives are more, and the single-objective performance by the a, c and d parameter factor levels of the degree of influence is different, if the direct manual selection of the parameter factor levels of the value of the parameter factor level will have a large error, so the variance can be used to determine the optimization variables on the optimization of the objective of the influence of the weight, and then obtain a reasonable combination of the parameter factor levels.

The size of the variance can characterize the degree of deviation of the data from the average value, through the analysis of the variance can know the optimization variables in each optimization objective influence weight, according to the size of the weight, can determine the optimization variables that have a greater influence weight on each optimization objective. Calculate the variance according to equation 8:

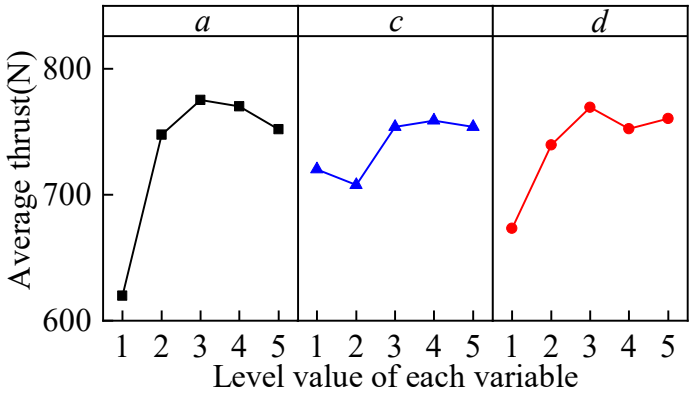

(a) Average thrust

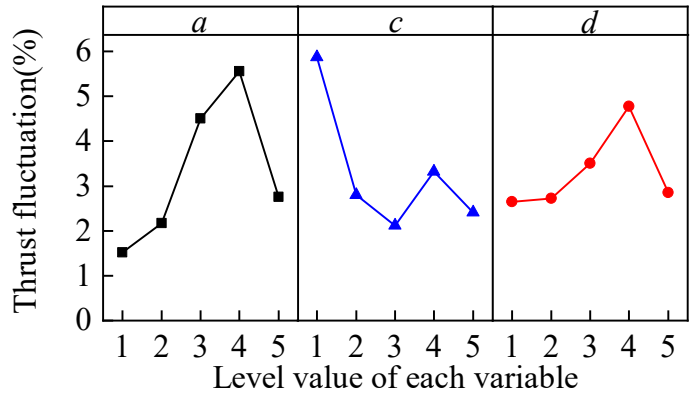

(b) thrust fluctuation

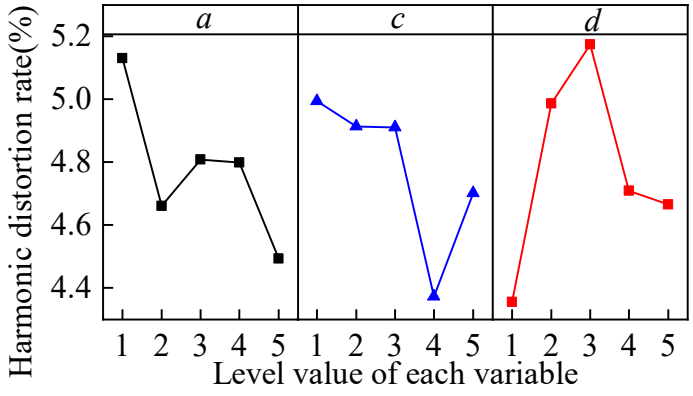

(c) No-load reverse potential harmonic distortion rate

Figure 8. Optimize Target Performance Averages

$$S_X = \frac{1}{n}\sum_{i=1}^{n}\left(X_{\delta(l)}\text{-}X_{avg}\right)^2. \tag{8}$$

Table 5. Variance And Weight Of Each Parameter Performance Indicator At Each Factor Level

Parameters	F_{avg}/N		K_R/%		K_T/%	
	variance	Specific gravity /%	variance	Specific gravity	variance	Specific gravity
a	3633.43	69.33	2.25	47.95	0.044	25.34
c	433.43	8.27	1.81	38.60	0.051	29.06
d	1174.29	22.41	0.63	13.45	0.079	45.60
Total	5241.15	100	4.69	100	0.174	100

Where X_{avg} is the average value of each optimization objective in Table 4 under the total number of experiments. The results of calculating the variance and weight of each parameter performance indicator at each factor level are shown in Table 5.

From Table 5, it can be seen that the optimization variables affect the weight order of each optimization objective respectively, for the average thrust, the parameter *a*>*d*>*c*; for the thrust fluctuation, the parameter *a*>*c*>*d*; and for the no-load counterpotential harmonic distortion rate, the parameter *d*>*c*>*a*.

3.3. Comparative Analysis of Optimization Results

In determining the optimal parameter factor level combinations, the value of parameter a is determined by the maximum average thrust and the minimum thrust fluctuation, the value of parameter d is determined by the minimum no-load counterpotential harmonic distortion rate, and the value of parameter c is determined by the criterion of smaller thrust fluctuation. According to the weight of the influence of optimization variables on the optimization objective, the final optimized level combination of each parameter factor is *a*(3)*c*(5)*d*(3), and the value of each parameter factor is *a*(0.31)*c*(9)*d*(0.37).

According to the values of each parameter of the final optimization scheme, finite element comparison is used to verify the electromagnetic performance of SU-PMLVM before and after optimization, and the thrust waveform and no-load counterpotential harmonic analysis are shown in Fig.10 and Fig.11, respectively, which shows that the performance of average thrust, thrust fluctuation, and no-load counterpotential harmonic distortion rate are improved compared with that of the pre-optimization. Table 6 shows the comparison of the performance of the motor before and after optimization.

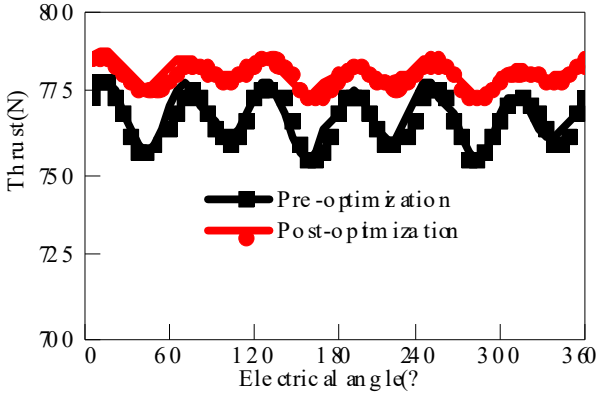

Figure 9. Thrust Waveform Comparison Before And After Optimization

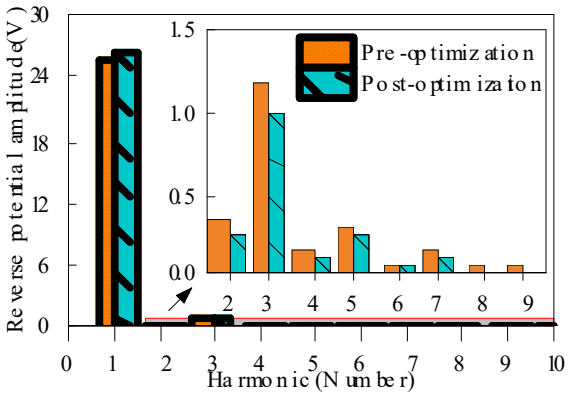

Figure 10. No-Load Reverse Potential Harmonic Analysis Before And After Optimization

Table 6. The Values of Each Parameter Before And After Optimization

Performance indicators	pre-optimization	post-optimization	variations
Average thrust /N	767.70	781.26	+13.56
Thrust fluctuation /%	3.12	1.87	-1.51
Reverse potential harmonic distortion rate /%	4.86	4.12	-0.74
Reverse potential amplitude /V	24.73	25.30	+0.57

4. SUMMARY

In this paper, a six-phase U-type permanent magnet linear vernier motor is proposed, and in order to further improve the comprehensive performance of SU-PMLVM, Taguchi's method is used to optimize the design of the motor structural parameters a, c, and d with the optimization objectives of average thrust, thrust fluctuation, and no-load counterpotential harmonic distortion rate. Comparing the performance of the motor before and after optimization, the thrust fluctuation of the optimized motor decreases from 3.11% to 1.87% with a decrease of 40.06%, the average thrust increases from 767.70N to 781.26N with an increase of 1.77%, the no-load back-potential harmonic distortion rate decreases from 4.86% to 4.12% with a decrease of 15.23%, and the no-load back-potential amplitude increases by 2.30%. The rationality of the proposed SU-PMLVM design and the effectiveness of its optimization method are verified.

REFERENCES

[1] Boduroglu, A., Demir, Y., Cu mhur, B., et al. (2021). A Novel Track Structure of Double-Sided Linear PM Synchronous Motor for Low Cost and High Force Density Applications. IEEE Transactions on Magnetics, 57(2) , 1-5. DOI:10.1109/TMAG.2020.3017448.

[2] Zhou, You., Shi, Chaojie., Qu, Ronghai., et al. (2021). Overview of Flux-modulation Linear Permanent Magnet Machines. Proceedings of the CSEE, 41(4),1469-1484. DOI: 10.13334/j.0258-8013.pcsee.201567.

[3] Wang, H., Gu, C., Wang, S., et al. (2023). Single-Phase Short-Circuit Fault Tolerant Control for Five-Phase Permanent Magnet Machines with Copper Loss Reduction. IEEE Transactions on Industrial Electronics, 70(11), 11087-11097. DOI: 10.1109/TIE.2022.3231322.

[4] Shi, Yujunl., Cheng, Zihuo., Jian, Linni. (2021). Comparative Analysis of Two Typical Field Modulated Permanent-Magnet Machines. Transactions Of China Electrotechnical society, 36(01), 120-130. DOI: 10.19595/j.cnki.1000-6753.tces.191108.

[5] Ishikawa, R., Sato, K., Shimomura, S., et al. (2013). Design of in-wheel permanent magnet vernier machine to reduce the armature current density. IEEE Proceedings of the 2013 International Conference on Electrical Machines and Systems, 459-464. DOI: 10.1109/ICEMS.2013.6754567.

[6] Wang, Xiuping., Jian, Shenglong, Qu, Chunyu. (2023). Structural optimization design of Halbach array permanent magnet cursor motor. Electric Machines and Control, 27(4), 140-147. DOI: 10.15938/j.emc.2023.04.014.

[7] Y, Du., K, Chau., M, Cheng., et al. (2011). Design and analysis of linear stator permanent magnet vernier machines. IEEE Transactions on Magnetics, 47(10,4219-4222. DOI: 10.1109/TMAG.2011.2156392.

[8] Nick J, Baker., Mohammad A H, Raihan., et al. (2018). Evaluating Alternative Linear Vernier Hybrid Machine Topologies for Integration into Wave Energy Converters. IEEE Transactions on Energy Conversion, 33(4), 2007-2017. DOI: 10.1109/TEC.2018.2873913.

[9] J, Ji., W, Zhao., Z, Fang., et al. (2015). A novel linear permanent-magnet vernier machine with improved force performance. IEEE Transactions on Magnetics, 51(8), 8106710. DOI: 10.1109/TMAG.2015.2416123.

[10] Wenxiang. Zhao., Tian. Yao., Liang. Xu., et al. (2021). Multi-Objective Optimization Design of a Modular Linear Permanent-Magnet Vernier Machine by Combined Approximation Models and Differential Evolution. IEEE Transactions on Industrial Electronics, 68(6), 4634-4645. DOI: 10.1109/TIE.2020.2988233.

[11] Liu, Zhiyou., Zhou, Haibo., Wang, Xiao-Ling., et al. (2018). Design and analysis of micro linear-rotary voice coil motor. Transducer and Microsystem Technologies, 37(07), 90-91+95. DOI: 10.13873/j.1000-9787(2018)07-0090-02.

[12] Li, Shuaiyao., Li, Jia-Chun., Chen, Bo., et al. (2024). Design and optimization analysis of outer rotor permanent magnet motor inside hoist. Manufacturing Automation, 46(01),120-124+129.

[13] Xu, Hai., Xu, Meng., Zhou, Yuxiang., et al. (2023). Ontology optimization of switched reluctance motor based on improved particle swarm optimization algorithm. Journal of Electronic Measurement and Instrument. 37(04), 131-141. DOI: 10.13382/j.jemi.B2206140.

[14] Han, Yandong., Wang, Xudong., Xu, Xiaozhuo., et al. (2016). PID control of permanent magnet linear synchronous motor based on genetic algorithms. Electronic Measurement Technology, 39(5), 115-119. DOI:10. 19651/ j. cnki. emt. 2016.05.026.

[15] Dai, Rui., Zhang, Yue., Wang, Huijun., et al. (2022). Optimal Design of Dual 12-phase High Speed Permanent Magnet Rectified Generator Based on Kriging Model. Proceedings of the CSEE, 42(2), 818-827. DOI:10. 13334/ j. 0258-8013.pcsee.201980.

[16] Cheng. Peng., Yang. Xinjiu., Lan. Hai., et al. (2019). Design and efficiency optimization of a synchronous generator using finite element method and Taguchi method. Electric Machines and Control, 23(02), 94-99,104. DOI: 10. 15938/ j.emc.2019.02.012.

[17] Fan, Zhaoyang., Ai, Liwang. (2023).Multi-objective optimal design of sector magnetic pole linear vernier motor. Transducer and Microsystem Technologies, 42, 91-94,99. DOI:10.13873/J.1000-9787(2023)05-0091-04.

[18] Cheng, Ming., Han, Peng., Hua, Wei. (2017). General airgap field modulation theory for electrical machines. IEEE Transactions on Industrial Electronics, 64(8), 6063-6074. DOI: 10.1109/TIE.2017.2682792.